

PAPER

Attaining the shot-noise-limit in the ACME measurement of the electron electric dipole moment

To cite this article: C D Panda *et al* 2019 *J. Phys. B: At. Mol. Opt. Phys.* **52** 235003

View the [article online](#) for updates and enhancements.

Recent citations

- [The metastable \$Q^3\$ state of ThO: a new resource for the ACME electron EDM search](#)
X Wu *et al*







IOP | ebooks™

Bringing you innovative digital publishing with leading voices to create your essential collection of books in STEM research.

Start exploring the collection - download the first chapter of every title for free.

Attaining the shot-noise-limit in the ACME measurement of the electron electric dipole moment

C D Panda^{1,5} , C Meisenholder¹ , M Verma², D G Ang¹ , J Chow³, Z Lasner³, X Wu^{1,3} , D DeMille³, J M Doyle¹ and G Gabrielse⁴

¹Department of Physics, Harvard University, Cambridge, MA 02138, United States of America

²Department of Physics, University of Toronto, Toronto, Ontario M5S 1A7, Canada

³Department of Physics, Yale University, New Haven, CT 06511, United States of America

⁴Center for Fundamental Physics, Northwestern University, Evanston, IL 60208, United States of America

E-mail: cristian.panda@gmail.com

Received 1 July 2019, revised 12 September 2019

Accepted for publication 2 October 2019

Published 4 November 2019



Abstract

Experimental searches for the electron electric dipole moment, d_e , probe new physics beyond the Standard Model. Recently, the ACME Collaboration set a new limit of $|d_e| < 1.1 \times 10^{-29} e \cdot \text{cm}$ (ACME Collaboration 2018 *Nature* **562** 355–60), constraining time reversal symmetry (T) violating physics in the 3–100 TeV energy scale. ACME extracts d_e from the measurement of electron spin precession due to the thorium monoxide (ThO) molecule's internal electric field. This recent ACME II measurement achieved an order of magnitude increased sensitivity over ACME I by reducing both statistical and systematic uncertainties in the measurement of the electric dipole precession frequency. The ACME II statistical uncertainty was a factor of 1.7 above the ideal shot-noise limit. We have since traced this excess noise to timing imperfections. When the experimental imperfections are eliminated, we show that shot noise limit is attained by acquiring noise-free data in the same configuration as ACME II.

Keywords: electron electric dipole moment, beyond the standard model, shot-noise limit, spin precession measurement, excess noise suppression, fast polarization switching

(Some figures may appear in colour only in the online journal)

Introduction

The electric dipole moment of the electron, \vec{d}_e , is an asymmetric charge distribution along the particle's spin, \vec{s} . Theories of physics beyond the Standard Model often include new particles with masses of 3–100 TeV/ c^2 whose interaction with the electron include T-violating phases and lead to $d_e \approx 10^{-27} - 10^{-30} e \cdot \text{cm}$ [1–7], orders of magnitude higher than the value predicted by the Standard Model, which is at the level of $d_e \lesssim 10^{-38} e \cdot \text{cm}$ [8, 9]. Measurements of d_e with increased precision probe for new physics in this energy range [10].

Recent advances in the measurement of d_e [10–14] have relied on the exceptionally high internal effective electric field \mathcal{E}_{eff} of heavy polar molecules. We perform our measurement in the $\text{H}^3\Delta_1$ state of ThO, which provides $\mathcal{E}_{\text{eff}} = 78 \text{ GV cm}^{-1}$ [15, 16]. In the presence of d_e , this gives rise to an energy shift $U = -\vec{d}_e \cdot \vec{\mathcal{E}}_{\text{eff}}$.

We measure this energy shift U by observing electron spin precession in parallel uniform applied electric ($\vec{\mathcal{E}} = \mathcal{E}\hat{z}$) and magnetic fields ($\vec{\mathcal{B}} = \mathcal{B}\hat{z}$) (figure 1(a)). We control the spin of the $\text{H}^3\Delta_1$ molecular state, \vec{S} , which is proportional to the spin of the electron \vec{s} . \vec{S} and \vec{s} correspond to the expectation values for our large ensemble of their quantum mechanical operators. To initialize the measurement, we use a linearly polarized laser propagating along \hat{z} , the axis of the applied fields $\vec{\mathcal{E}}$ and $\vec{\mathcal{B}}$, to align \vec{S} along the fixed direction

⁵ Author to whom any correspondence should be addressed.

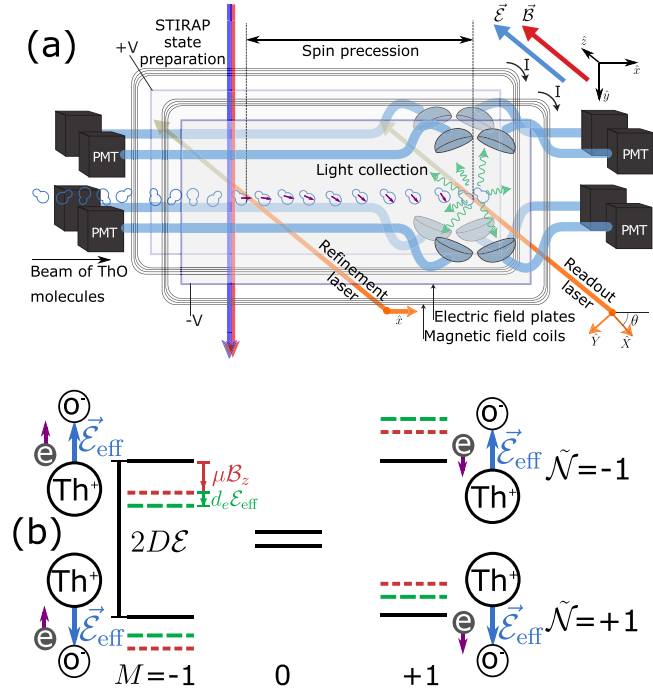


Figure 1. Schematic of the ACME II measurement region and level diagram. (a) A ThO spin state aligned along \hat{x} (purple arrows), prepared by stimulated Raman adiabatic passage (STIRAP) and refined via an optical pumping laser beam polarized along \hat{x} (left orange arrow), precesses in applied electric ($\vec{\mathcal{E}}$, blue arrow) and magnetic ($\vec{\mathcal{B}}$, red arrow) fields. The final spin alignment direction is read out by a laser with rapidly alternating linear polarizations (right orange arrow), $\hat{\varepsilon} = \hat{X}, \hat{Y}$ (with the former at an angle θ with respect to \hat{x}). The resulting fluorescence (green wavy arrows), whose intensity depends on the angle between \vec{S} and $\hat{\varepsilon}$, is collected and detected with photomultiplier tubes (PMTs). (b) H, $J = 1$, state levels in external $\vec{\mathcal{E}}$ and $\vec{\mathcal{B}}$ fields, accompanied by cartoons depicting the orientation of the effective electric field $\vec{\mathcal{E}}_{\text{eff}}$ (blue arrows) and the spin of the electron \vec{s} (purple arrows). The energy shifts $\mu\mathcal{B}_z$ (red) and $d_e\mathcal{E}_{\text{eff}}$ (green) due to the magnetic moment μ and the EDM d_e , respectively, are shown. The $\tilde{N} = \pm 1$ states are split by $2D\mathcal{E} \sim 200$ MHz due to the Stark effect.

given by the polarization of the laser light [10, 17]. The \vec{S} vector is in the xy plane and perpendicular to \hat{z} .

We allow \vec{S} to precess under the torques of the applied magnetic field $\vec{\mathcal{B}}$ and $\vec{\mathcal{E}}_{\text{eff}}$ on the magnetic and electric dipole moments associated with \vec{S} . We measure the precession angle $\phi = \omega\tau$, where the precession frequency is

$$\omega \approx \frac{-\mu\tilde{\mathcal{B}}|\mathcal{B}_z| - \tilde{N}\tilde{\mathcal{E}}d_e\mathcal{E}_{\text{eff}}}{\hbar}, \quad (1)$$

and τ is the spin precession time, $|\mathcal{B}_z| = |\vec{\mathcal{B}} \cdot \hat{z}|$, $\tilde{\mathcal{B}} = \text{sgn}(\vec{\mathcal{B}} \cdot \hat{z})$, $\tilde{\mathcal{E}} = \text{sgn}(\vec{\mathcal{E}} \cdot \hat{z})$, and $\mu = \mu_B g_H$, where $g_H = -0.0044$ is the g -factor of the H, $J = 1$ state [18] and μ_B is the Bohr magneton. We extract the precession time, τ , from the change of ϕ that comes from reversing the applied magnetic field, $\phi^{\mathcal{B}} = -\mu|\mathcal{B}_z|\tau/\hbar$. We then compute the angular precession frequency, $\omega = \phi/\tau$.

We use pairs of states in the H $^3\Delta_1$ manifold that correspond to $\vec{\mathcal{E}}_{\text{eff}}$ being aligned and anti-aligned with the applied $\vec{\mathcal{E}}$, labeled by the quantum number $\tilde{N} = \text{sgn}(\vec{\mathcal{E}}_{\text{eff}} \cdot \vec{\mathcal{E}})$

(figure 1(b)). These states are spectroscopically resolved, and tuning our lasers to be resonant with either $\tilde{N} = \pm 1$ allows us to reverse the direction of $\vec{\mathcal{E}}_{\text{eff}}$ independently of the direction of $\vec{\mathcal{E}}$. To extract the contribution of d_e to ω , we reverse the direction of $\vec{\mathcal{E}}_{\text{eff}}$ either by reversing the laboratory field $\vec{\mathcal{E}}$ or by changing the state $\tilde{N} = \pm 1$ used in the measurement. By denoting this contribution as $\omega^{\tilde{N}\mathcal{E}}$, we obtain $d_e = -\hbar\omega^{\tilde{N}\mathcal{E}}/\mathcal{E}_{\text{eff}}$.

The standard quantum limit for the uncertainty in the measurement of d_e is determined by shot noise: that is, for N detected molecules, $\delta_{d_e}^{s-n} = (2\tau\mathcal{E}_{\text{eff}}\sqrt{N})^{-1}$ [12]. However, technical noise sources can make $\delta_{d_e} > \delta_{d_e}^{s-n}$ [18]. Unfortunately, a previously unidentified source produced a form of technical noise that increased the ACME II statistical uncertainty in the measurement of d_e by a factor of 1.7 above shot noise. In this work we trace this excess noise to imperfect hardware timing. We verify that the excess noise was accounted for appropriately in the ACME II analysis. We also show that with the timing imperfections under control, the shot noise limit can be attained. Eliminating this error will allow future ACME measurements to obtain higher sensitivity.

Measurement of the precession frequency through fast polarization switching

We measure the precession frequency ω by exciting the H–I transition with laser light (703 nm) linearly polarized along direction $\hat{\varepsilon}$. This yields fluorescence signals with intensity $S_{\hat{\varepsilon}}$, which depends on the angle between $\hat{\varepsilon}$ and \vec{S} . To remove excess technical noise due to fluctuations in molecule number, we excite the molecules with two alternating orthogonal linear polarizations, $\hat{\varepsilon} = \hat{X}, \hat{Y}$, by modulating $\hat{\varepsilon}$ sufficiently rapidly (period $5\mu\text{s}$) so that each molecule is addressed by both polarizations as it passes through the laser beam [10, 12]. We record the corresponding fluorescence signals $S_X(t)$ and $S_Y(t)$ from the decay of I to the ground state X (wavelength 512 nm; see figure 2), as a function of time within the polarization switching cycle, t .

In ACME II, fluorescence was recorded using a data acquisition (DAQ) digitizer⁶ operating at a sampling rate of 16 MSA s^{-1} . At this sampling rate, each acquired sample contained signal integrated over $T_{\text{dig}} = 62.5$ ns. Each polarization switching cycle (period $T = 5\mu\text{s}$) contained 80 samples, with the first (last) 40 assigned to signals with polarization \hat{X} (\hat{Y}). We labeled the digitized signals at each point as S_X^i (S_Y^i), where $i \in \{1, 2, 3 \dots 40\}$ labels the digitization point starting at time $t_i = (i-1)T_{\text{dig}}$. The first point in the polarization cycle, S_X^1 , was chosen consistently throughout the analysis as the point where the \hat{X} laser turns on, i.e. the first point where $S_X > 0$. We computed integrated fluorescence signals by summing over samples within a chosen region of time between when a given polarization is turned on and when the next polarization is turned on, sb , which we

⁶ NI PXI-5171R FPGA.

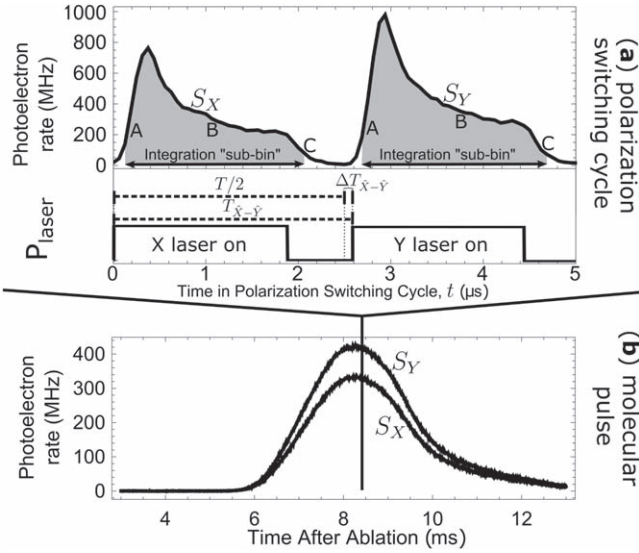


Figure 2. Switching timescales. (a) Fluorescence signal size versus time in an \hat{X} , \hat{Y} polarization cycle. The integration ‘sub-bin’ typically used in ACME II is shown in gray. $T_{\hat{X}-\hat{Y}}$ is the time delay between the \hat{X} and \hat{Y} laser pulses. $\Delta T_{\hat{X}-\hat{Y}} = T_{\hat{X}-\hat{Y}} - T/2$ is the asymmetric relative time delay between the optical \hat{X} , \hat{Y} pulses. A, B, and C denote regions of distinct quantum state population dynamics. (b) Measured molecular fluorescence signal trace (25 pulses averaged) versus time. Shown signals are averaged over the entire \hat{X} and \hat{Y} polarization cycles from (a).

referred to as an integration ‘sub-bin’ (see figure 2)

$$S_X = \sum_{i \in sb} S_X^i \quad \left(S_Y = \sum_{i \in sb} S_Y^i \right). \quad (2)$$

The ‘sub-bin’ is common to both \hat{X} and \hat{Y} polarization cycles. Typically, we used $sb = \{3, 4, 5 \dots 34\}$ in ACME II. Typical ACME II integrated fluorescence signals plotted as a function of time after ablation are shown in figure 2(b).

We then compute the asymmetry

$$\mathcal{A} = \frac{S_X - S_Y}{S_X + S_Y} = \mathcal{C} \cos[2(\phi - \theta)], \quad (3)$$

where the contrast \mathcal{C} is $95\% \pm 2\%$ on average and \hat{X} is defined to be at an angle θ with respect to the horizontal lab axis \hat{x} in the x - y plane. We measure \mathcal{C} by dithering θ between two nearby values, $\tilde{\theta} = \pm 1$, that differ by 0.2 rad (11.5°). We then compute the precession frequency,

$$\omega = \frac{\phi}{\tau} = \frac{\mathcal{A}}{2\mathcal{C}\tau}, \quad (4)$$

from the asymmetry, \mathcal{A} , contrast, \mathcal{C} , and precession time, τ .

To implement the fast polarization switching scheme experimentally, we overlap two laser beams with orthogonal \hat{X} and \hat{Y} polarizations, which we switch alternatively on and off rapidly using acousto-optical modulators (AOMs) [12, 19]. The two beams are combined on a polarizing beamsplitter which rejects any possible polarization imperfections. In ACME II, the \hat{X} and \hat{Y} pulses each had a duration of 1.9 μs , with a nominal 0.6 μs delay between them. Given the 115 ns lifetime of the I state (figure 2), this delay was sufficient to reduce the overlap between fluorescence signals arising from excitation by the different laser polarizations.

The shape of the time-modulated fluorescence signal, $S(t)$, is given by the quantum state population dynamics resulting from the properties of the readout molecular states H and I, and the laser beam intensity spatial and time profiles. Immediately after the laser is switched on, there is a rapid increase in fluorescence as molecules in the laser beam are quickly excited (region A in figure 2). When $\Omega_r t \ll 1$, where $\Omega_r \sim 2\pi \times 3$ MHz is the Rabi frequency of the readout H–I transition, the fluorescence magnitude increases as $S(t) \propto \Omega_r^2 t^2$. Later, when $\Omega_r t \geq 1$, population is roughly evenly mixed between the H and I states, causing $S(t)$ to decay nearly exponentially with a time constant of $2\tau_I$ (region B in figure 2), where $\tau_I \approx 115$ ns is the lifetime of the I state. During the time the laser is on, molecules continually enter the laser beam, such that the nearly exponential decay approaches a constant fluorescence rate in the steady state. After the laser turns off, the signal decays exponentially with time constant τ_I (region C in figure 2).

One important parameter in this polarization switching scheme is the time delay between the \hat{X} and \hat{Y} laser pulses, $T_{\hat{X}-\hat{Y}}$ (figure 2). Ideally, $T_{\hat{X}-\hat{Y}} = T/2$, where T is the polarization switching period ($T = 5$ μs in ACME II). However, since the laser intensity modulation is performed by AOMs, there is an additional delay in the timing of the \hat{X} , \hat{Y} optical pulses relative to the electronic trigger pulses due to the propagation time of the acoustic wave in the acousto-optic crystal [20, 21]. This propagation delay is sensitive to the alignment and spatial intensity profile of the laser beam and the geometry of the specific AOM crystal used. We found that in our apparatus, it could vary due to manual realignment of the laser beam through the AOM by up to 200 ns. Such alignment was typically done every several days during ACME II.

During ACME II, we corrected for this additional relative delay between the \hat{X} , \hat{Y} optical pulses by manually adding in the experiment timing structure a time delay between the \hat{X} , \hat{Y} electronic trigger pulses, such that the asymmetric relative time delay between the optical \hat{X} , \hat{Y} pulses, $\Delta T_{\hat{X}-\hat{Y}} = T_{\hat{X}-\hat{Y}} - T/2$, is minimized, i.e. $\Delta T_{\hat{X}-\hat{Y}} \approx 0$. This was implemented during ACME II by observing both \hat{X} and \hat{Y} optical pulses on the same photodiode and matching the optical dead-times between the signals. Using this technique, we could set $\Delta T_{\hat{X}-\hat{Y}} = 0$ with ~ 40 ns precision, better than the timing corresponding to one digitizer sample (62.5 ns). However, we show below that even this imprecision in setting $\Delta T_{\hat{X}-\hat{Y}} = 0$ is important; with any nonzero residual value, the asymmetry acquires a dependence on time within the polarization switching cycle that can cause frequency noise when combined with technical timing noise.

Frequency noise in ACME II

During the ACME II measurement sequence, we performed a set of 7 binary switches of experimental parameters⁷ that

⁷ The switches in a superblock are described in [10], but the details are unimportant here.

allowed us to compute the frequency component due to $d_e, \omega^{N\mathcal{E}}$. The time scales of the switches ranged from the fastest (0.6 s) to slowest (10 min). Each set of 2^7 states (~ 20 min acquisition time), corresponding to the 7 switches, represented a ‘superblock’.

During data acquisition, we averaged 25 molecular pulses together to form a ‘trace’ (0.5 s averaging time). Within a trace, we computed \mathcal{A} for each polarization cycle. We then averaged 20 consecutive cycles into a single ‘group,’ with uncertainty defined as the standard error in the mean of the group. The uncertainties of each group were consistent with the level due to shot noise on our photoelectron signals. We then used standard uncertainty propagation to compute uncertainties from an entire superblock.

The ACME II dataset consisted of ~ 1000 superblocks acquired over a period of 2 months. The majority of the data was consistent with a distribution nearly Gaussian near its center, but with an excess of points in the tails [10]. In addition, the scatter in the superblock data was found to be larger than expected from group-level uncertainties. The excess noise was present equally in all 2^7 states of the experiment. Furthermore, the relative magnitude of the noise with respect to shot-noise did not vary as a function of time within the molecular pulse. The excess noise in the precession frequency had one contribution that was proportional to the \mathcal{B} -field magnitude, and another that was independent of \mathcal{B} . We discuss the two separately.

We quantify the magnitude of the noise by computing the reduced chi-square per degree of freedom of the dataset, χ_r^2 . The \mathcal{B} -field dependent component of the excess noise increased the scatter of the ACME II superblock data to $\chi_r^2 \sim 7$, for data acquired at the largest applied \mathcal{B} -field magnitude, $|\mathcal{B}_z| = 26$ mG. As described previously [10], we reduced this noise contribution by acquiring most data at lower magnetic field magnitudes, $|\mathcal{B}_z| \in \{0.7, 1.3, 2.6\}$ mG, where the associated increase in χ_r^2 is negligible.

We focus the discussion in this paper on the \mathcal{B} -independent component of excess noise, which limited the sensitivity of ACME II. The statistical uncertainty was ~ 1.7 times larger than that expected from shot-noise, corresponding to a reduced chi-squared statistic of the superblock data of $\chi_r^2 \sim 3$.

Diagnosis of excess noise sources

To characterize this excess noise source, we perform a noise diagnosis in an experimental setup that is similar to ACME II, but without actually executing any of the 7 binary switches. Furthermore, we perform our analysis on data from single molecular pulses, rather than averaging 25 consecutive pulses in a ‘trace’, as was done in ACME II. This allows us to observe the properties of our measurement directly at fast timescales, before switching and averaging obscure important underlying characteristics of our measurement that we ultimately found were leading to frequency noise.

Mechanism causing variable trigger-to-digitizer delays

Using this diagnosis method, we found that one ingredient that causes frequency noise is variation in the triggering of the acquisition of the individual molecular pulses. Such variation can occur in our system due to a lack of synchronization between the signals triggering the polarization switching AOMs and those triggering the DAQ digitizer. In ACME II, a common high precision timing and delay generator⁸ provided TTL pulses that acted as triggers for the RF switches that modulated the polarization switching AOMs on and off. The same pulse generator acted as a trigger for the digitization sequence. These two trigger signals were phase locked to suppress their relative timing jitter to < 25 ps.

However, during this diagnosis of noise sources, we find that the synchronization of the laser polarization pulses with the DAQ digitization events was not, in fact, consistent with the low jitter between these trigger pulses. The reason is that our particular DAQ digitizer uses an internal clock to perform the timing of the sampling and digitization process, rather than responding directly to an external trigger. Hence, if the timing generator and the DAQ internal clock are not explicitly synchronized, there is an uncontrolled delay between the DAQ acquisition trigger pulse and the actual start of digitization.

During ACME II, this asynchrony caused molecular pulses to have their digitization begin with varying time delays relative to the AOM triggers controlling the $\hat{X} - \hat{Y}$ polarization switch, with magnitude of up to ~ 100 ns. Each subsequent molecular pulse (triggered at a rate of 50 Hz) was deterministically offset from the previous by ~ 10 ns. This timing offset is consistent with the inaccuracy (5×10^{-7}) of the internal clock of the DAQ device. When the delay reached ~ 100 ns (every 10 molecular pulses), it reset to 0, creating a periodic sawtooth pattern.

For the current tests, we eliminate this varying trigger-to-digitizer delay by using an external clock⁹ to synchronize the electronic signals triggering the polarization switching AOMs with the internal clock of the DAQ digitizer. However, proper synchronization of the DAQ digitizer to an external clock also required a firmware update of the digitizer. This originally made the noise difficult to identify. Furthermore, low-jitter synchronization (< 25 ps) between experiment timing and actual digitization events is only possible when the digitizer’s sampling rate is set to be an integer divisor of the 250 MSa s^{-1} internal clock rate. This was not the case in ACME II, where the digitizer sampling rate was set to 16 MSa s^{-1} .

To achieve minimum timing variation between digitization events and polarization switching, we implement a modified timing structure from that used in ACME II. We choose a 12.5 MSa s^{-1} digitization rate in these tests, commensurate with the digitizer’s internal clock rate. (Faster rates are not possible in the current setup due to the limited data transfer rate of the computer system performing the acquisition.) At this sampling rate, each acquired sample contains

⁸ SRS DG645.

⁹ 10 MHz from a Rubidium reference clock, SRS FS725.

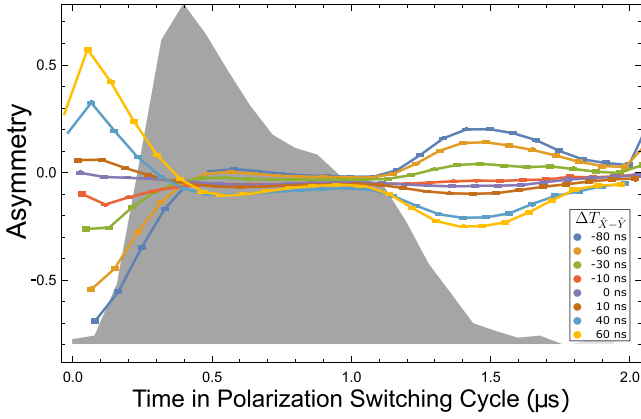


Figure 3. Asymmetry, $\mathcal{A}(t)$, versus time in polarization switching cycle, for various values of $\Delta T_{\hat{X}-\hat{Y}}$. The average signal, $S(t)$, is shown in gray. The magnitude of $\mathcal{A}(t)$ at any given time is proportional to the asymmetric \hat{X} , \hat{Y} pulse time delay parameter, $\Delta T_{\hat{X}-\hat{Y}}$, and to the slope of the fluorescence signal in the polarization bin, $dS(t)/dt$. The asymmetries shown here are calculated by averaging 200 consecutive molecular pulses (4 s averaging time).

signal integrated over 80 ns (compared to 62.5 ns in ACME II). To ensure an even number of digitization samples in a polarization switching cycle, we set the polarization switching frequency to 250 kHz (compared to 200 kHz in ACME II), such that each full polarization cycle contains exactly 50 digitizer samples, 25 corresponding to the \hat{X} and \hat{Y} polarization bins, respectively. The dead-time between the \hat{X} and \hat{Y} halves of the polarization cycle, when both laser polarizations are off, is set to 0.8 μs (0.6 μs in ACME II).

Asymmetry dependence on $\Delta T_{\hat{X}-\hat{Y}}$

As described above, for ACME II, we typically computed a ‘time-averaged’ asymmetry by averaging the digitizer samples in the chosen integration ‘sub-bin,’ defined in the same way for both \hat{X} and \hat{Y} halves of the polarization cycle. In contrast, we analyze the data used for the noise tests described here by calculating the asymmetry for each single acquired digitizer sample in the \hat{X} and \hat{Y} bins:

$$\mathcal{A}^i = \frac{S_X^i - S_Y^i}{S_X^i + S_Y^i}, \quad (5)$$

where now $i \in \{1, 2, 3, \dots, 25\}$ due to the new full polarization switching period ($T = 4 \mu\text{s}$) and new digitization rate (12.5 MSa s^{-1}). This results in asymmetry values which we use to show the dependence of the noise and asymmetry offset on the time in the polarization switching cycle.

Figure 3 shows the asymmetry, $\mathcal{A}^i = \mathcal{A}(t_i)$, as a function of time in the polarization switching cycle. We observe that the asymmetric relative time delay between the optical \hat{X} , \hat{Y} pulses, $\Delta T_{\hat{X}-\hat{Y}}$ (see figure 2), has a large effect on the shape and magnitude of the resulting asymmetry and its dependence on time within the polarization cycle. This occurs because when $\Delta T_{\hat{X}-\hat{Y}} \neq 0$, there is a difference in the acquisition times of $S_X(t_i)$ and $S_Y(t_i)$ relative to when the laser light with that polarization is switched on. This causes the computed

asymmetry within the polarization switching cycle, $\mathcal{A}(t_i)$, which should nominally be constant, to have a time-dependent difference from its mean, $\Delta\mathcal{A}(t)$. When $\Delta T_{\hat{X}-\hat{Y}} \ll T$, we can approximate this variation in the asymmetry as

$$\Delta\mathcal{A}(t) \approx \frac{1}{2S(t)} \frac{dS(t)}{dt} \Delta T_{\hat{X}-\hat{Y}}, \quad (6)$$

where $S(t)$ is the signal averaged over the \hat{X} and \hat{Y} polarizations, $S(t) = (S_X(t) + S_Y(t))/2$.

We note that $\Delta\mathcal{A}(t)$ is independent of any of the experiment switches performed routinely as a part of the ACME II superblock structure. Therefore, in the channels of interest in the experiment, all of which are odd under at least one of these switches, offsets due to $\Delta\mathcal{A}(t)$ are cancelled. In particular, we have searched for and not observed any systematic variation of the $\omega^{\mathcal{N}^\mathcal{E}}$ frequency, or any of the other odd frequency channels, correlated with time within the polarization switching cycle [22]. In addition, the $\hat{\mathcal{P}}$ and $\hat{\mathcal{R}}$ switches (described in detail in [12]) each interchange the roles of the \hat{X} and \hat{Y} readout laser beams [10, 12], reversing the sign of the asymmetry: $\mathcal{A}(t) \xrightarrow{\hat{\mathcal{P}}, \hat{\mathcal{R}}} -\mathcal{A}(t)$. This transformation subtracts $\Delta\mathcal{A}(t)$ in the $\hat{\mathcal{P}}$, $\hat{\mathcal{R}}$ -even channels (such as the $\omega^{\mathcal{N}^\mathcal{E}}$ channel, which is used to compute d_e), so that on average the presence of $\Delta\mathcal{A}(t)$ cannot systematically shift the measurement of ϕ and ω .

Technical variable trigger-to-digitizer delays lead to asymmetry noise

This dependence of asymmetry on time within the polarization switching cycle can, however, cause noise in the asymmetry. This arises when such a non-zero $\Delta\mathcal{A}(t)$ is present together with a variation in the trigger-to-digitizer delay relative to the start of the polarization switching laser pulses. This noise appears not only in the raw asymmetry, but also leaks into the channels which are odd with respect to the performed switches, if the variation of the trigger timing takes place on time scales shorter than the fastest experimental switch defining any such channel. For example, any $\tilde{\mathcal{N}}$ -odd switch parity signal will exhibit this noise if the trigger timing varies on timescales that are faster than the $\tilde{\mathcal{N}}$ experiment switch (every 0.6 s). This is shown in figures 4(a) and (b), when there is a large amount of timing variance (as present during the ACME II dataset) or with reduced technical timing variance, respectively. We achieve the two configurations by either making commensurate or not the DAQ internal clock and the external clock that defines the polarization switching times, as described above. When the clocks are not commensurate, the noise also propagates equally into all computed odd and even switch channels since the technical timing variation timescale (≈ 10 pulses = 0.2 s) is faster than the timescale of the fastest experiment switch $\tilde{\mathcal{N}}$ (0.6 s).

In the presence of large timing variation, the computed χ_r^2 for the set of 200 molecular pulses is largest at the beginning and end of the polarization switching optical pulse. The data is consistent with our model (equation (6)), where noise is proportional to the time dependent asymmetry shown

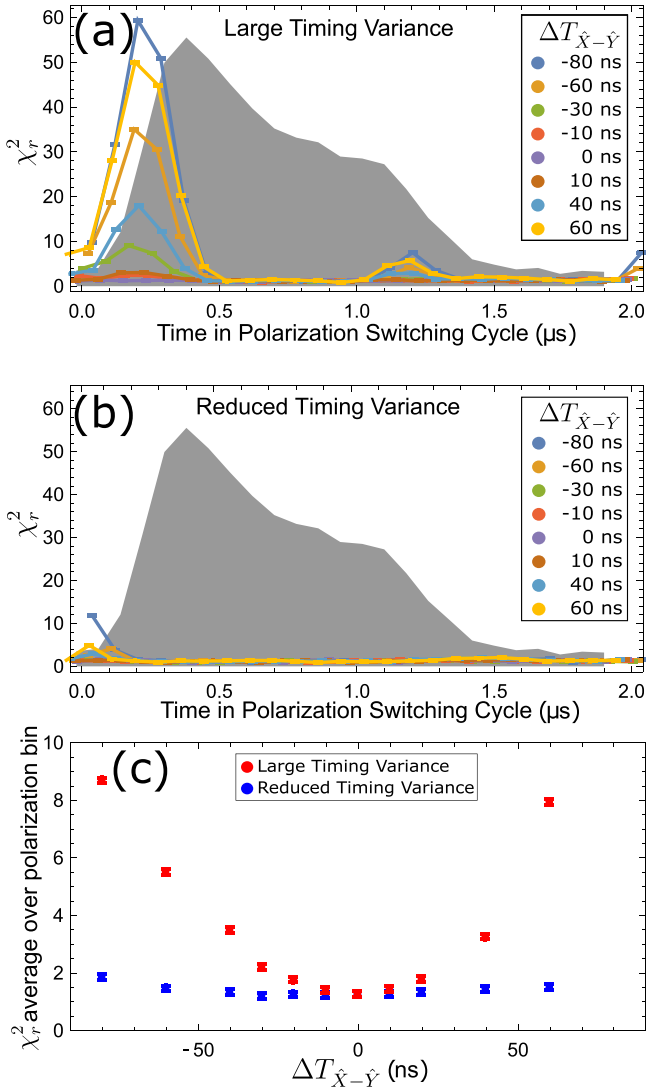


Figure 4. Variation of asymmetry noise within the polarization bin with $\Delta T_{\hat{x}-\hat{y}}$. Measured magnitude of excess noise, parameterized by χ_r^2 , versus time within the polarization switching cycle, for various values of $\Delta T_{\hat{x}-\hat{y}}$, (a) with large timing noise, and (b) when timing noise is reduced. The noise is larger where the slope of the fluorescence signal ($S(t)$ shown in gray), $dS(t)/dt$, is larger. (c) χ_r^2 averaged over the entire time in the polarization switching cycle, shown as a function of $\Delta T_{\hat{x}-\hat{y}}$, for large timing variance and when timing variance is reduced. All χ_r^2 values are calculated for 200 consecutive molecular pulses, acquired over 4 s.

in figure 3, $\chi_r^2 \propto \Delta A(t)^2 \propto \left(\frac{dS(t)}{dt} \Delta T_{\hat{x}-\hat{y}}\right)^2$. Figure 4(c) shows χ_r^2 averaged over the entire polarization cycle (integration ‘sub-bin’ $sb = \{1, 2, \dots, 25\}$) as a function of $\Delta T_{\hat{x}-\hat{y}}$, in the presence of timing variance and with timing variance reduced. This demonstrates the reduced magnitude of noise with lower timing variance and when $\Delta T_{\hat{x}-\hat{y}} = 0$.

Control and suppression of noise

With the noise mechanism understood, we reduce the magnitude of the excess noise by suppressing the experiment

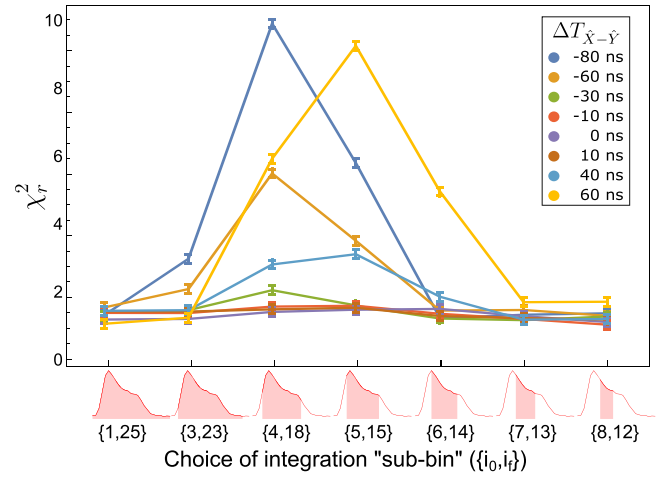


Figure 5. Dependence of the excess noise on choice of integration sub-bin. The noise (χ_r^2) is reduced when the integration sub-bin is chosen such that it does not begin or end with the samples with largest amount of excess noise. This behavior is consistent for all values of $\Delta T_{\hat{x}-\hat{y}}$. The shown data is acquired in the ‘large timing noise’ configuration, where the clocks of the timing box and DAQ digitizer are not synchronized. All χ_r^2 values are calculated for 200 consecutive molecular pulses, acquired over 4 s.

imperfections that contribute to it. As shown in figure 4(c), we can reduce the noise by suppressing DAQ timing variance and/or setting $\Delta T_{\hat{x}-\hat{y}}$ to zero. Each of these parameters can be suppressed by several orders of magnitude compared to values that were typical in ACME II. Since the suppression is multiplicative, this source of noise can be greatly reduced in future ACME experiments.

A third method could also be used to further suppress this source of frequency noise if necessary. As shown in equation (6), $\Delta A(t)$ is proportional to the slope of the signal, dS/dt . When summed over the entire ‘sub-bin’, as typically done during ACME II data analysis, ΔA is only a function of signals at the beginning and end of the ‘sub-bin’ integration time: $\Delta A = \int_{i_0}^{i_f} \Delta A(t) dt$, where i_0 and i_f are the first and last indexes in the integration ‘sub-bin’. There is no dependence of ΔA on the intermediary points, i.e. for $i_0 < i < i_f$. This means that the noise can be minimized if we choose the ‘sub-bin’ such that variation in signal at both the start and end times, S^{i_0} , S^{i_f} are minimized. This behavior is shown in figure 5.

Finally, we verified the suppression of the asymmetry noise when using all three methods simultaneously (minimized $\Delta T_{\hat{x}-\hat{y}}$, reduced timing variance, using a full ‘sub-bin’ of $sb = \{1, 2, \dots, 25\}$). Under these conditions, we acquired 12 superblocs of data with the same sets of switches and parameters as in the ACME II experiment. This produced data consistent with a Gaussian distribution out to its tails with $\chi_r^2 = 0.87 \pm 0.40$, consistent with 1. This confirmed the suppression of this (and any other) sources of noise to below the ACME II shot-noise limited statistical uncertainty.

A further alternative method of suppressing such noise in the future is by performing one of the experimental switches that changes the sign of the signals of interest at a timescale that is faster than that of any timing variation. This can be

achieved, for example, by using the \tilde{P} switch, which is currently implemented using AOMs and could be performed at a faster timescale. Another option is performing the \tilde{N} switch at faster timescales. We could, for example, switch \tilde{N} every molecular pulse, 25 times faster than in ACME II.

Conclusion

We have understood and quantified a technical timing variation mechanism that accounts for the excess noise present in the ACME II measurement of d_e . The mechanism which added unbiased noise to the measurement of the asymmetry was due to a combination of timing variance between the DAQ digitizer and polarization switching events, and an asymmetric relative time delay between the \hat{X} and \hat{Y} polarization switching optical pulses. Such noise mechanisms can be a concern for experiments that, like ACME, compare different experimental states by rapidly switching between them.

We showed here that the noise can be suppressed by reducing the two timing imperfections that contribute to it and by integrating over a larger sub-bin within the polarization switching signal. We verified suppression to a level below the ACME II experiment shot-noise limited sensitivity, by acquiring noise-free data in the same configuration as ACME II. The noise reduction represents a factor of 1.7 increase in the statistical sensitivity of future ACME experiments, compared to ACME II, for this effect alone. Based on the model for its origin, we expect that this source of technical noise is suppressed by several orders of magnitude below its ACME II level.

Acknowledgments

This work was performed as part of the ACME Collaboration, to whom we are grateful for its contributions, and was supported by the NSF.

ORCID iDs

C D Panda  <https://orcid.org/0000-0002-2284-9756>
 C Meisenhelder  <https://orcid.org/0000-0002-0339-5672>
 D G Ang  <https://orcid.org/0000-0002-7501-7507>
 X Wu  <https://orcid.org/0000-0002-6646-820X>

References

- [1] Cesarotti C, Lu Q, Nakai Y, Parikh A and Reece M 2019 *J. High Energy Phys.* **2019** 59
- [2] Fuyuto K, Ramsey-Musolf M and Shen T 2019 *Phys. Lett. B* **788** 52–7
- [3] Nakai Y and Reece M 2017 *J. High Energy Phys.* **2017** 31
- [4] Barr S M 1993 *Int. J. Mod. Phys. A* **08** 209–36
- [5] Pospelov M and Ritz A 2005 *Ann. Phys.* **318** 119–69
- [6] Engel J, Ramsey-Musolf M J and van Kolck U 2013 *Prog. Part. Nucl. Phys.* **71** 21–74
- [7] Bernreuther W and Suzuki M 1991 *Rev. Mod. Phys.* **63** 313–40
- [8] Pospelov M E and Khriplovich I B 1991 *Sov. J. Nucl. Phys.* **53** 638–40
- [9] Pospelov M and Ritz A 2014 *Phys. Rev. D* **89** 1–7
- [10] ACME Collaboration 2018 *Nature* **562** 355–60
- [11] Baron J *et al* 2014 *Science* **343** 269–72
- [12] ACME Collaboration 2016 *New J. Phys.* **19** 073029
- [13] Cairncross W B, Gresh D N, Grau M, Cossel K C, Roussy T S, Ni Y, Zhou Y, Ye J and Cornell E A 2017 *Phys. Rev. Lett.* **119** 1–5
- [14] Kara D M, Smallman I J, Hudson J J, Sauer B E, Tarbutt M R and Hinds E A 2012 *New J. Phys.* **14** 103051
- [15] Denis M and Fleig T 2016 *J. Chem. Phys.* **145** 214307
- [16] Skripnikov L V 2016 *J. Chem. Phys.* **145** 214301
- [17] Panda C D *et al* 2016 *Phys. Rev. A* **93** 1–9
- [18] Kirilov E *et al* 2013 *Phys. Rev. A* **88** 013844
- [19] Vutha A C *et al* 2010 *J. Phys. B: At. Mol. Opt. Phys.* **43** 074007
- [20] Degenhardt C, Nazarova T, Lisdat C, Stoehr H, Sterr U and Riehle F 2005 *IEEE Trans. Instrum. Meas.* **54** 771–5
- [21] Falke S, Misera M, Sterr U and Lisdat C 2012 *Appl. Phys. B* **107** 301–11
- [22] Panda C D 2018 Order of magnitude improved limit on the electric dipole moment of the electron *PhD Thesis* Harvard University